Available online at www.sciencedirect.com
SCIENCE DIRECT®
Nuclear Engineering and Design 235 (2005) 1875–1887
Nuclear Engineering and Design
www.elsevier.com/locate/nucengdes

Wavelet time–frequency analysis of accelerating and decelerating flows in a tube bank

M.L.S. Indrusiak, J.V. Goulart, C.R. Olinto, S.V. Möller *

Programa de Pós-Graduação em Engenharia Mecânica-PROMEC, Universidade Federal do Rio Grande do Sul-UFRGS, Rua Sarmento Leite 425, 90050-170 Porto Alegre, RS, Brazil

Received 18 November 2004; received in revised form 24 May 2005; accepted 30 May 2005

Abstract

In the present work, the steady approximation for accelerating and decelerating flows through tube banks is discussed. With this purpose, the experimental study of velocity and pressure fluctuations of transient turbulent cross-flow in a tube bank with square arrangement and a pitch-to-diameter ratio of 1.26 is performed. The Reynolds number at steady-state flow, computed with the tube diameter and the flow velocity in the narrow gap between the tubes, is 8×10^4. Air is the working fluid. The accelerating and decelerating transients are obtained by means of start and stop of the centrifugal blower. Wavelet and wavelet packet multiresolution analysis were applied to decompose the signal in frequency intervals, using Daubechies 20 wavelet and scale functions, thus allowing the analysis of phenomena in a time–frequency domain. The continuous wavelet transform was also applied, using the Morlet function. The signals in the steady state, which presented a bistable behavior, were separated in two modes and analyzed with usual statistic tools. The results were compared with the steady-state assumption, demonstrating the ability of wavelets for analyzing time varying signals.

1. Introduction

Banks of tubes or rods are found in the nuclear and process industries, being the most common geometry used in heat exchangers. Attempts to increase heat exchange ratios in heat transfer equipments do not consider, as a priority of project criteria, structural effects caused by the turbulent fluid flow, unless failures occur (Païdoussis, 1982). By attempting to improve the heat transfer process, dynamic loads are increased and may produce vibration of the structures, leading, generally, to fatigue cracks and fretting-wear damage of the components, which are one of the failure sources affecting nuclear power plant performance (Pettigrew et al., 1998).

Pressure fluctuations result from velocity fluctuations at several points of the flow field (Willmarth, 1975). They are produced by the interaction of velocity gradients with velocity fluctuations and Reynolds

* Corresponding author. Tel.: +55 51 33163228; fax: +55 51 33164001.
E-mail address: svmoller@ufrgs.br (S.V. Möller).
URL: www.mecanica.ufrgs.br/lmf.

0029-5493/$ – see front matter © 2005 Elsevier B.V. All rights reserved.
doi:10.1016/j.nucengdes.2005.05.029

Nomenclature

a	scale index
$a_{j,k}$	approximation coefficient [$g(t)$]
b	position index
$d_{j,k}$	detail coefficient [$g(t)$]
D	diameter (m)
f	frequency (Hz)
$g(t)$, $h(t)$	generic time functions [$g(t)$, $h(t)$]
j	dilation index
k	translation index
p	pressure (Pa)
P	pitch (m)
$P_{gg}(a, b)$	wavelet spectrum $[g(t)]^2$
$P_{gh}(a, b)$	wavelet cross-spectrum $[g(t)\cdot h(t)]$
P/D	aspect ratio
Re	Reynolds number: $Re = U\cdot D/\nu$
Sr	Strouhal number, $Sr = f\cdot D/U$
t	time (s)
U, v	velocities ($m\,s^{-1}$)
U_{app}	incidence velocity ($m\,s^{-1}$)
$W_g(a, b)$, $W_h(a, b)$	continuous wavelet transform coefficients [$g(t)$, $h(t)$]
$W_g^*(a, b)$, $W_h^*(a, b)$	complex conjugate of $W_g(a, b)$, $W_h(a, b)$ [$g(t)$, $h(t)$]

Greek letters

$\phi_{a,b}(t)$, $\phi_{j,k}(t)$	scaling functions
ν	kinematic viscosity ($m^2\,s^{-1}$)
$\psi_{a,b}(t)$, $\psi_{j,k}(t)$	wavelet functions

stresses (Rotta, 1972). The amplitude of the pressure fluctuations may be influenced by velocity fluctuations at a distance comparable to the wavelength of these fluctuations (Townsend, 1976). The search of form and magnitude of pressure and velocity fluctuations and the interdependence between these quantities is necessary for the comprehension of the complex phenomena in tube banks, since the resulting forces applied to the tubes by the turbulent flow will be given by the integral of the pressure field around each tube in the bank. From the fluctuating pressure field, a fluctuating excitation force will result, which may induce vibration of the tube if its natural frequency is present in the excitation force (Blevins, 1990).

The concern about heat transfer equipment integrity is, therefore, due to the close relationship between fluid flow around a solid surface and the vibrations induced by the flow in the structure by wall pressure fluctuations.

The classic approach to these studies is the Fourier analysis, which can give information about the frequencies involved and the interdependence of simultaneous phenomena (e.g. velocity and pressure fluctuations at different locations). An ergodic hypothesis of the time series is necessary in this case, being mean values independent of the sampling process. This hypothesis fails in time varying series, which means that Fourier analysis cannot deal with a signal that is changing over time and, therefore, its mean values are not constant. Furthermore, many processes of interest in fluid dynamics are not stationary. In accelerating flows, for instance, beside their mean values not being constant, additional phenomena may appear, as the flow velocity changes with time.

Unsteady flows occur frequently in nuclear and process installations, due to reciprocating pumps, water hammer phenomenon and process control. Analysis of such flows is often based on a quasi-steady approximation, with the transient phenomena being considered as having the same characteristics to those of steady flow at the same instantaneous Reynolds number. Nevertheless, dynamic loads like those produced by vortex shedding and other hydrodynamic processes, like fluid elastic instabilities, turbulent buffeting and acoustic resonance should be investigated under transient conditions.

The modern literature presents the wavelets as a tool to analyze such class of problems, including time varying series and discontinuities in this series. The purpose of this paper is to explore the use of wavelets in the study of unsteady turbulent flows through tube banks. The unsteady flow condition is obtained by accelerating and decelerating the flow.

2. Background

2.1. Fourier spectral analysis

Spectral analysis is a modification of the Fourier analysis, more suitable for random time functions than for deterministic functions. A generic time function

$g(t)$ is represented in Fourier domain by coefficients obtained from the inner products of $g(t)$ with the Fourier basis. The auto spectral density function (PSD) of a random time series is the squared Fourier coefficients of that series smoothed over frequency intervals and over an ensemble of estimates, in order to minimize the random error (Bendat and Piersol, 1971).

2.2. Wavelet analysis

Wavelet analysis is similar to Fourier analysis in that the original function is expanded over an orthogonal basis. The Fourier basis is a set of sinusoidal functions and the wavelet basis is a set formed by dilations and translations of a single function called wavelet.

A wavelet can be described as a wavy function carefully constructed so that it grows and decays in a limited time period (Ogden, 1997; Percival and Walden, 2000). A wavelet function tends to zero as time goes to infinity and integrates to zero while its square integrates to unity. In the last years, many different wavelets were developed (Meyer, 1993). The function developed by Haar in 1910 is considered the most suitable to the introduction and of the understanding of wavelet analysis.

Denoting the scale as a and the position as b, the continuous wavelet basis is given by:

$$\psi_{a,b}(t) = \frac{1}{\sqrt{a}}\psi\left(\frac{t-b}{a}\right) \tag{1}$$

The continuous wavelet transform of a discrete time function $g(t)$ is given by:

$$W_g(a,b) = \int_t g(t)\psi_{a,b}(t)\,\mathrm{d}t \tag{2}$$

The respective wavelet spectrum is:

$$P_{gg}(a,b) = |W_g(a,b)|^2 \tag{3}$$

While the auto spectral density function or Fourier spectrum gives the energy for each frequency over the entire time domain, in the wavelet spectrum (equation (3)), the energy is related to each time and scale (or frequency). This characteristic of the wavelet transform allows the representation of the distribution of the energy of the transient signal over time–frequency domains.

The continuous wavelet cross-spectrum of two discrete time functions $g(t)$ and $h(t)$ is:

$$P_{gh}(a,b) = W_g(a,b)W_h^*(a,b) \tag{4}$$

where $W_h^*(a,b)$ is the complex conjugate of the continuous wavelet transform of $h(t)$. The absolute values of $P_{gh}(a,b)$ give information about the coherence between the two signals in time–frequency domain, more detailed than the analysis of both the cross-spectrum and the cross-correlation in Fourier space.

To have a discrete wavelet basis, a and b are replaced, respectively, by 2^j and $k2^j$, where j and k are the so-called dyadic dilation and translation indexes, thus

$$\psi_{j,k}(t) = 2^{-j/2}\psi(2^{-j}t - k) \tag{5}$$

A 2^N long time series is expressed in a discrete wavelet basis as:

$$g(t) = \sum_{j=0}^{N}\sum_{k=1}^{2^{N-j}} d_{j,k}\psi_{j,k}(t) \tag{6}$$

where, as in Fourier analysis, the wavelet or detail coefficients $d_{j,k}$ are simply the inner products of $g(t)$ with the corresponding basis functions.

Associated to each wavelet there is a scaling function, which also produces an orthogonal basis by means of dilations and translations:

$$\phi_{j,k}(t) = 2^{-j/2}\phi(2^{-j}t - k) \tag{7}$$

A jth degree smoothed time series can be obtained combining the set $\{\phi_{j,k},\ k=1,\ \ldots,\ 2^{N-j}\}$ with the scaling or approximation coefficients $a_{j,k}$ given by the inner products of $g(t)$ with the corresponding basis scaling functions:

$$g(t)_{j\text{th smooth}} = \sum_{k=1}^{2^{N-j}} a_{j,k}\phi_{j,k}(t) \tag{8}$$

All the sets $\{\psi_{j,k}\}$ and $\{\phi_{j,k}\}$ are mutually orthogonal, therefore the function can be expressed as:

$$g(t) = \sum_k a_{J,k}\phi_{J,k}(t) + \sum_{j\le J}\sum_k d_{j,k}\psi_{j,k}(t) \tag{9}$$

where J is the index of the last decomposition level of interest, where the decomposition sequence, up to level N, is truncated.

For a 2^N point sample, the indexes vary as follows: $1 \leq j \leq J \leq N$ and $1 \leq k \leq 2^{N-j}$. In other words, a time series $g(t)$ can be written as a sum of a coarse scaling series and J increasingly fine detail series.

The choice of the best wavelet for a given problem is not straightforward. In some situations, the results are similar for most wavelets, while for other problems; the result of the analysis depends strongly on the wavelet type used. Basically, the best wavelet for the analysis of a certain problem will be chosen by its ability of enhancing features of the studied phenomena and by its filter capabilities. In this research work, Daubechies 'db20' (Daubechies, 1992) wavelet functions were selected following a best filtering criterion. For the continuous wavelet spectra, the Morlet function was used.

Wavelet analysis can be understood as a refinement of Fourier analysis. The Fourier transform describes an original function in terms of its frequency components, over its whole domain. But for describing a signal that is changing over time, the time–frequency localization of the signal features has to be known. In equation (6), the coefficients $d_{j,k}$ are related to the amplitudes and energy of the signal at a given position k, corresponding to instant $t = 2^j k\,\Delta t$ and a period $2^j\,\Delta t$, where Δt is the acquisition interval. Therefore, there is a vector of coefficients $\{d_{j,k}\}$ associated to each frequency interval $[1/(2^{j+1}\,\Delta t), 1/(2^j\,\Delta t)]$.

When used for signal processing, wavelet analysis has, as a first result, the detection of singularities, due to the fact that wavelet coefficients are very sensitive to discontinuities and abrupt behavior changes of the signal. The features of the signal are more visible at continuous wavelet analysis, but the discrete analysis needs less computing time and memory.

Each set of detail coefficients retains the information concerning to a definite frequency interval and the signal can be reconstructed separately for each one of these intervals. These sets $g_j(t)$, obtained from the inner sum of equation (6), are part of the original signal and point out the localized time behavior of the signal at the corresponding frequency interval. However, the width of the frequency interval depends on the decomposition level, being larger for higher frequencies.

To obtain narrower frequency intervals another wavelet decomposition procedure must be applied. Considering each detail coefficient vector as a series and decomposing that series using the same wavelet and scaling functions, two series with, respectively, lower and upper half width frequency intervals are obtained. This scheme, applied recursively at all levels, generates a "wavelet tree", and is called wavelet packet transform. Each wavelet packet transform is associated with a level j, and the jth level decomposes the frequency interval of the original signal $[0, f/2]$ into 2^j intervals of equal bandwidths (Percival and Walden, 2000).

The first advantage of this band pass filter action of wavelet packet decomposition is that, by reconstructing separately each frequency interval, the signal is analyzed in a time–frequency domain, which gives the localization in time of the occurrence of the frequency of a selected event.

3. Experimental technique

The test section is the same used in Endres and Möller (2001), being a 1370 mm long rectangular channel, with 146 mm height and a maximal width of 193 mm (Fig. 1(a)). Air, at room temperature, is the working fluid, driven by a centrifugal blower, passed by a diffuser and a set of honeycombs and screens, before reaching measurement location with about 1% turbulence intensity. After the screens, a Pitot tube was placed at a fixed position to measure the reference velocity for the experiments and for the calculation of the Reynolds number at the steady-state condition.

For measurements of velocity and velocity fluctuations, DANTEC constant temperature hot wire anemometers were applied. Single and double hot wire probes were applied. Single probes used have one wire perpendicular to the main flow. The double wire probe has one wire perpendicular to the main flow and a second wire inclined 45° to the main flow, so that two components of the velocity vector and their fluctuations could be measured simultaneously.

Wall pressure fluctuations were measured by ENDEVCO piezo-resistive pressure transducers, mounted inside the tubes and connected to a pressure tap drilled in a nylon support adjusted to the tube inner wall.

The tube bank investigated had a pitch-to-diameter ratio $P/D = 1.26$ and square arrangement. The tubes were rigid and not heated. The flow was perpendicular to tube axes.

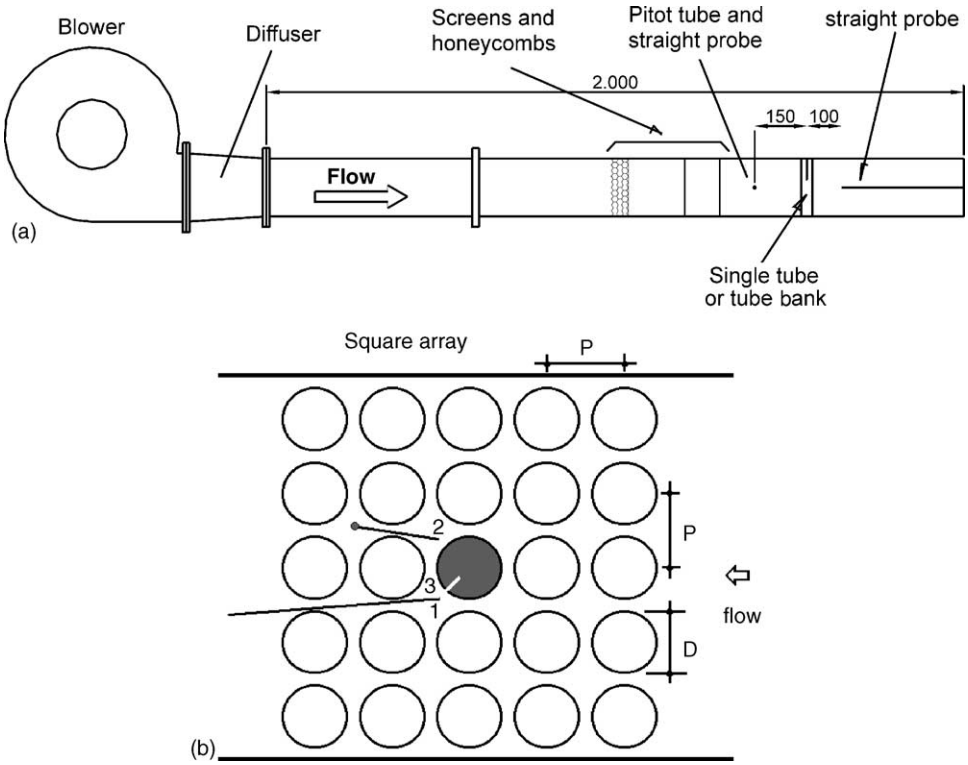

Fig. 1. Schematic view of the test section: (a) wind tunnel configuration and (b) tube bank with location of probes: (1 and 2) hot wires and (3) pressure tap for pressure transducer.

Fig. 1(b) shows schematic location of the probes in the tube bank. The support of hot wire "2" was fixed on the upper wall, while hot wire "1" was inserted from the outlet. The pressure transducer was installed in the central tube of the third row of the bank. All probes were placed at the same distance from upper and lower walls. The hot wires were positioned perpendicular to the tube axes.

Fig. 2 shows a scheme of the pressure transducer mounted inside the tube. The tube instrumented with the pressure transducer was the central one in the third row, as shown in Fig. 1(b).

The wall pressure in the region of central tube of the third row, where separation occurs, was acquired simultaneously with the velocities at both sides of the cylinder. Data acquisition of velocity and pressure were performed with a 12 bit Keithley DAS-58 A/D-converter board with sampling frequency of 25 kHz, and a low pass filter set at 10 kHz for velocity and 1.6 kHz for pressure. A sampling frequency of 8 kHz was also used, with low pass filters of 3 and 3.6 kHz, respectively, for velocity and pressure signals.

Time series were acquired in a transient flow, starting from rest and running to the stationary state, or from stationary state to rest, respectively, by turning the blower "on" or "off". Therefore, the Pitot tube could measure the velocity only in steady-state condition.

For reference, and to investigate the wavelet technique in transient flows, a first experiment was performed: two velocity components were acquired with the double wire probe in the wake of a single tube assembled perpendicular to the flow. The approaching velocity was simultaneously acquired with a single probe replacing the Pitot tube.

Wavelet analysis was performed using the Matlab 5.3 software.

Analysis of uncertainties in the results has a contribution of 1.4% from the measurement equipments (including hot wire and A/D converter). The mean error

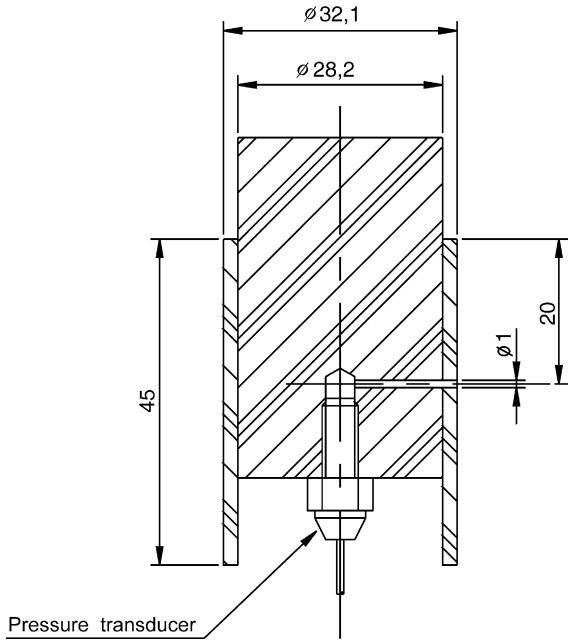

Fig. 2. Mounting scheme of the transducer support.

of the determination of the flow velocity with a hot wire is about 3.4%. Velocity fluctuations in the main flow direction are obtained with a mean error of 15%, while the transverse fluctuating component has an error of about 30%.

4. Results

Fig. 3(a) shows the transient signal acquired in the wake of a cylinder. The Reynolds number defined with the tube diameter and the stationary reference velocity was 3.1×10^4.

The power spectrum of the last half part of the vortex street series (Fig. 3(b)), where steady state is reached, shows a peak at about 104 Hz as the predominant frequency of vortex shedding in the wake. This corresponds to a Strouhal number, defined with the shedding frequency and the tube diameter of 0.22, about 5% higher then the classical value of 0.21. However, this value can be attributed to the blockage of the test section by the single tube (West and Apelt, 1982).

In order to analyze the vortex street development during acceleration of the flow, the transversal velocity

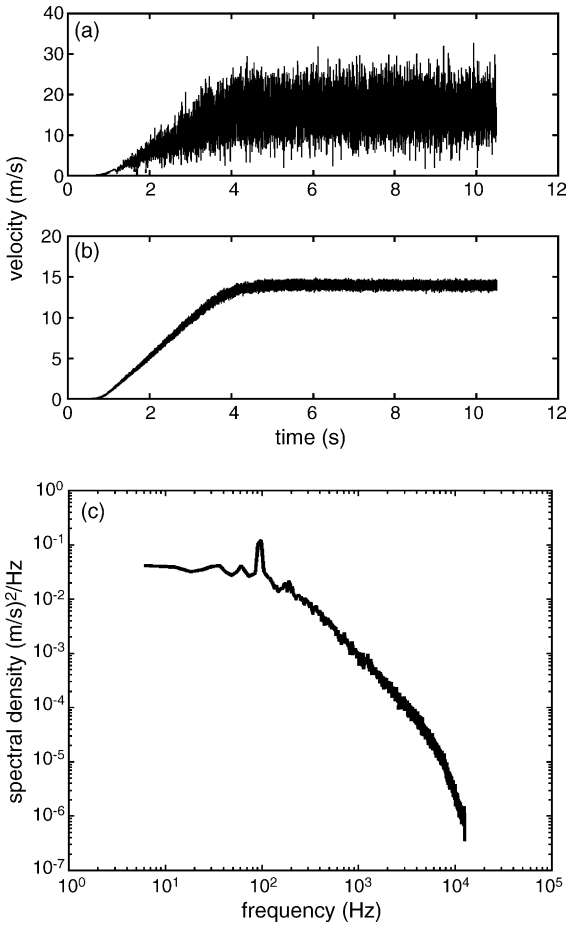

Fig. 3. Transient velocity in (a) the wake of a cylinder, (b) free stream reference velocity and (c) power spectrum of the stationary part of the vortex street series.

fluctuations perpendicular to both tube and tunnel axis was computed from the signals obtained by the double wire probe. An 11th level wavelet packet decomposition was applied to the time series, performing the so-called multiresolution analysis, and then the 11th level series were reconstructed, each with a bandwidth of 6.1 Hz. The results for some series were displayed in Fig. 4.

In the series of Fig. 4, the transient increase of amplitudes denotes the presence of the transient vortex shedding at the corresponding frequency interval and time. This occurs later for higher frequencies and, at the last frequency interval, from 103.7 to 109.8 Hz, the raise in the amplitude, which begins nearly at the onset

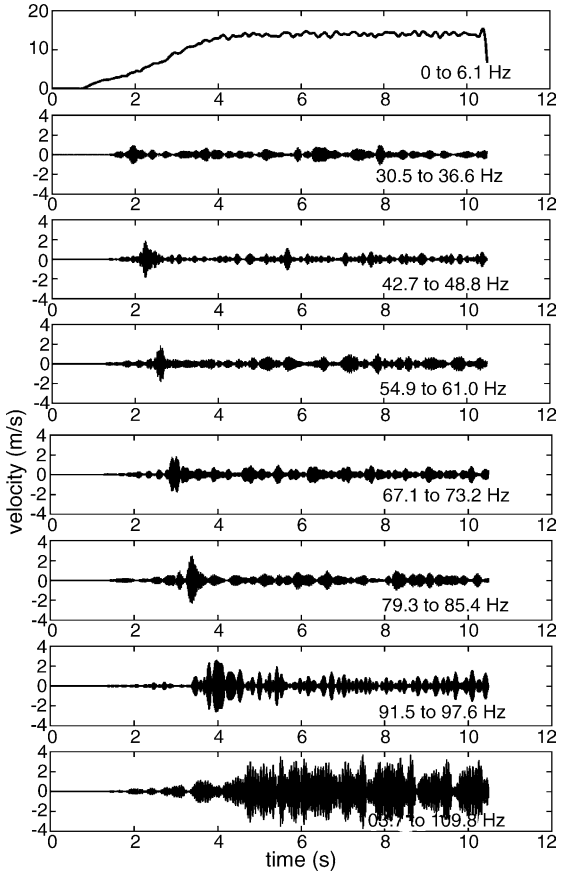

Fig. 4. Some reconstructed wavelet series for the transient velocity in the wake of a cylinder of Fig. 3(a) showing the time–frequency evolution of the wake.

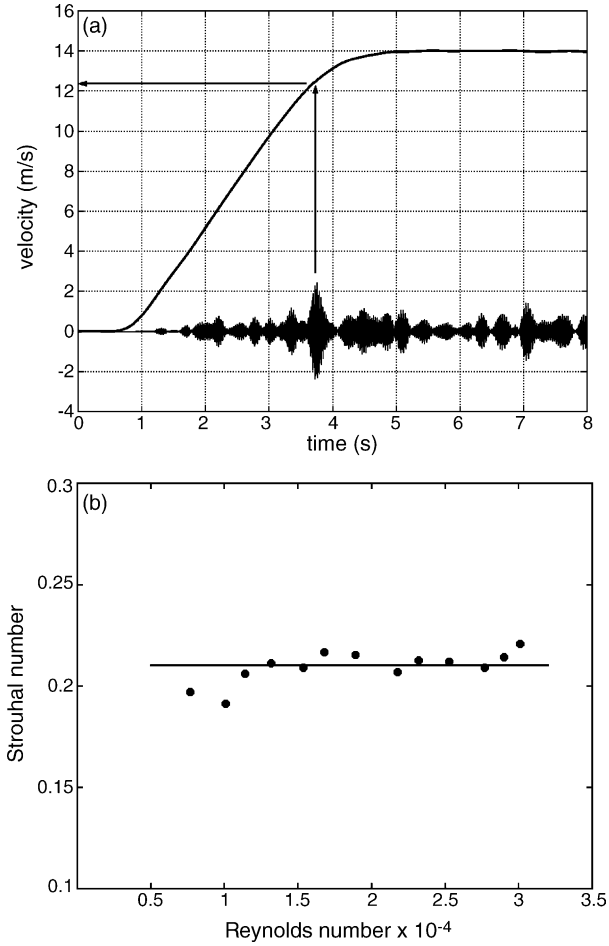

Fig. 5. (a) Time location of the transient vortex shedding and respective instantaneous mean approaching velocity, $\overline{U}_{app}$, for a generic frequency band. (b) Strouhal numbers, $Sr(t)$, computed from transient frequency and approaching velocity against Reynolds number based on tube diameter.

of stationary flow and holds until the end of the time series, denotes the presence of the stationary vortex shedding.

In order to relate the transient vortex shedding frequency and the free stream transient velocities approaching the cylinder, the mean point of transient increase of amplitudes was used to find the corresponding transient approaching velocity. The scheme shown in Fig. 5(a) illustrates this procedure, applied for each frequency interval, from 30.5 to 103.7 Hz. Some uncertainty in the determination of such points is due to the vortex shedding itself, which does not occur at a single distinct frequency, but rather it wanders over a narrow band of frequencies with a range of amplitudes (Blevins, 1990).

The transient Strouhal number can be evaluated as:

$$Sr(t) = \frac{\overline{f}_s(t)D}{\overline{U}_{app}(t)} \tag{10}$$

where D is the tube diameter, $\overline{U}_{app}$ the instantaneous mean approaching velocity and $\overline{f}_s$ is the mean frequency of the interval.

Fig. 5(b) shows the transient Strouhal number as a function of Reynolds number, which is approximately constant along time, the slight variations around 0.21 (continuous line) are due to the experimental inherent uncertainties.

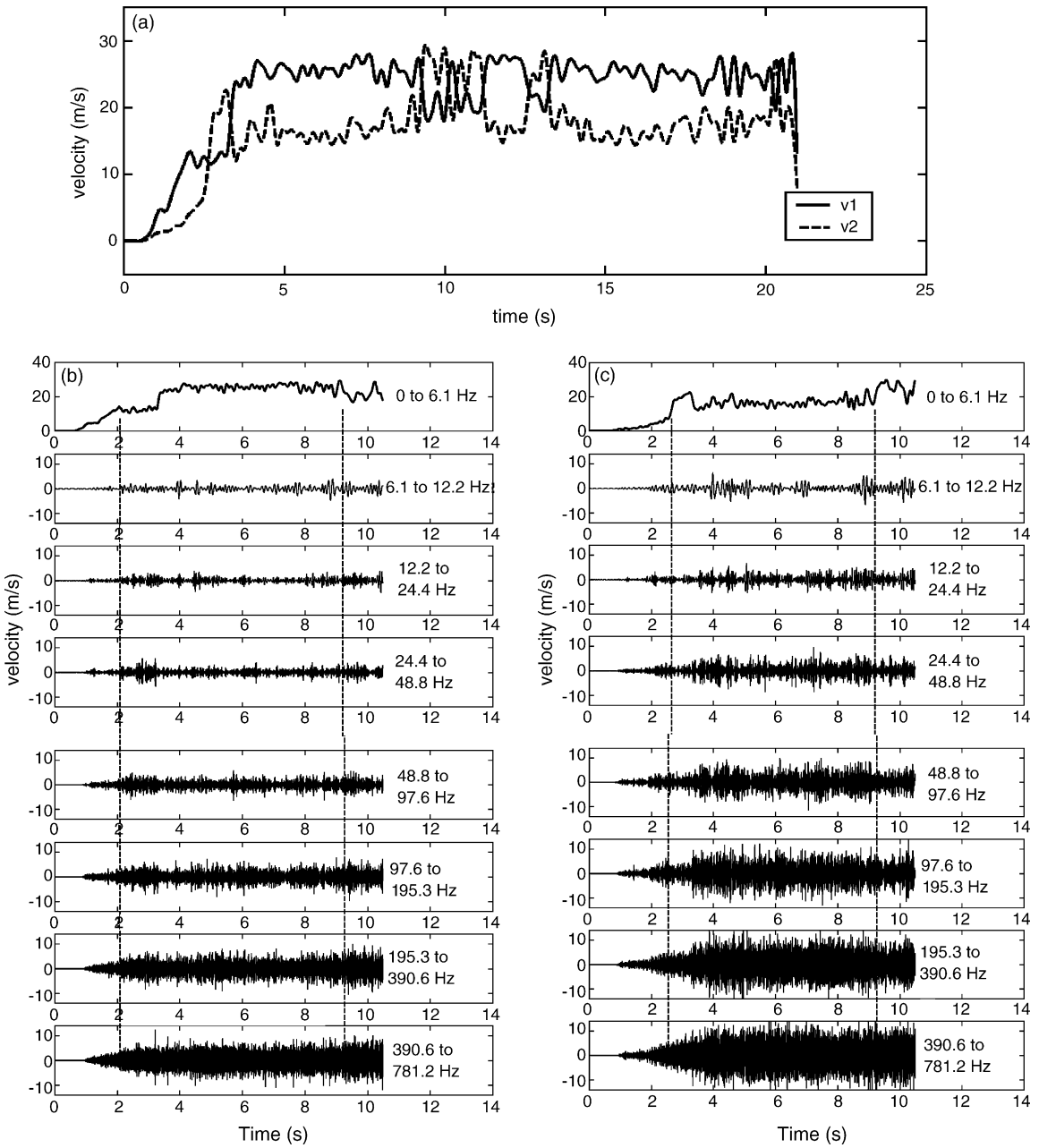

Fig. 6. (a) Wavelet approximation, corresponding to a 3 Hz low pass filter, of the velocity signals obtained from Probes "1" and "2". (b) Details from velocity signal of Probe "1". (c) Details from velocity signal of Probe "2".

The velocity signals acquired in the tube bank were analyzed with the continuous and discrete wavelet transforms. The 12th level reconstructed approximation sets Fig. 6(a) of the discrete wavelet transforms evidenced that the two signals alternate complementarily, at both transient and stationary parts, maintaining a regular mean velocity among them. The reconstructed detail sets (Fig. 6(b and c)) show that the fluctuations of the velocity are more intense at the time intervals corresponding to the lower mean velocity values and vice versa. Location of the probes is given by Fig. 1. In general, the velocity measured by Probe "2", which was nearer the tube wall than Probe "1" is lower than the velocity measured with Probe "1", but the turbulence intensity, evidenced by the amplitudes of the signal, is higher for Probe "2". This behavior seems to be more definite at lower frequencies, until 195 Hz.

To better observe this behavior, the continuous wavelet spectrum analysis of the first quarter part of the signal was made (Fig. 7). The gray scale used shows in darker gray the time–frequency localization of higher energy levels of the signal. It is noticeable that, at each interval, the velocity signal with the lower mean value has more energy at the fluctuations concerning the carrying energy vortices (lower frequencies). This is observed in Fig. 7(a), from about 3.3 s till the end of the record, and in Fig. 7(b), in the time interval between 2 and 3.3 s.

By decelerating the flow, by turning the blower off, it was expected to make the transient longer than at accelerating process and than to obtain more details about the transient process. This actually happened, but series longer than the capacity of the A/D converter were necessary, without giving substantive additional information.

More detailed results of pressure and velocity fluctuations for this geometry can be found in Endres and Möller (2001). According to Ziada et al. (1989), the pressure measurements provide no information about fluid periodicities in banks with in line tubes. The spectrum of velocity fluctuations can provide some information, if taken behind the first row, because the flow within the rest of the array becomes fully turbulent. The measurements shown in this paper, however, were

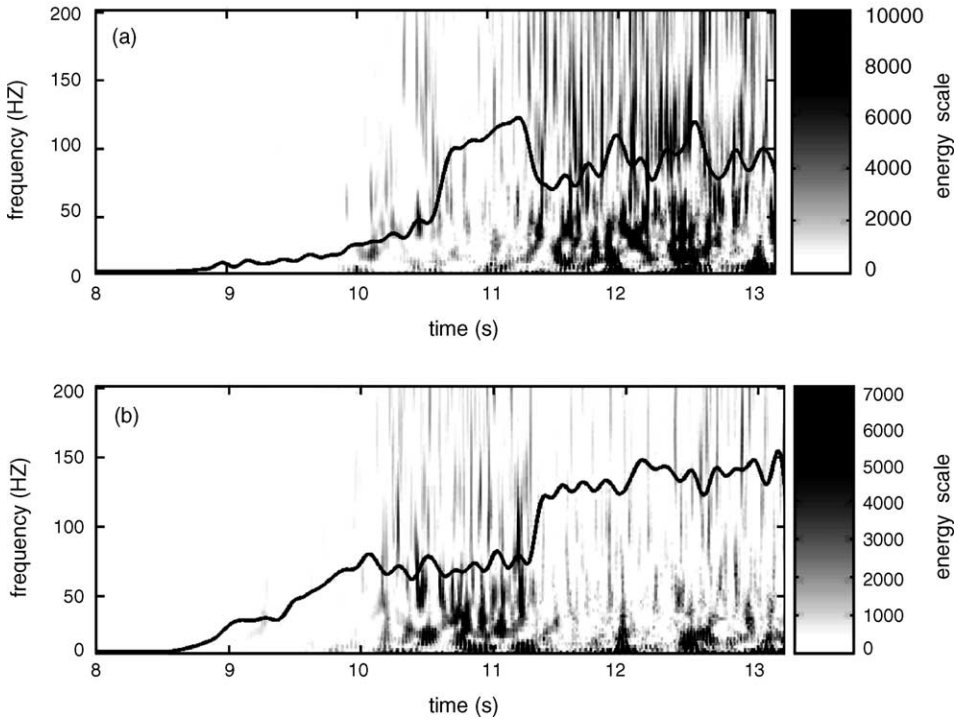

Fig. 7. Continuous wavelet spectrum of the velocity signals: (a) Probe "2" and (b) Probe "1".

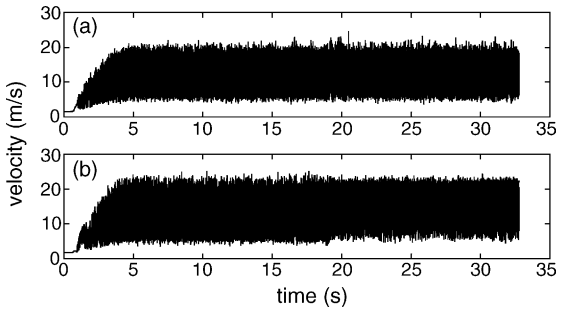

Fig. 8. Velocity signals of (a) Probe "1" and (b) Probe "2".

made behind the third row, and consequently, one can see only a fully turbulence spectrum, with no evidence of vortices shedding. Differently from large aspect ratio tube banks, where dynamic loads are mainly associated with the vortex shedding process, the turbulent flow in tube banks with small aspect ratios is characterized as broadband turbulence, without a defined shedding frequency (Blevins, 1990). In general, the behavior of spectra agrees with former results obtained in Endres and Möller (2001), for this geometry.

To study with more accuracy this unsteady behavior of the velocity that occurs even at stationary regime of the incident flow, several measurements at the same location were performed, using longer series and including the pressure signal. The series were acquired at 8 kHz and low pass filtered at 3 kHz for velocity and 3.6 kHz for pressure signals. Fig. 8 shows the velocity signals of a selected experiment. The signals seem to be stationary after 5 s, but the reconstructed approximations (Fig. 9), for a frequency interval of 0–4 Hz, show a strong change at 19 s, affecting both velocity signals and also the pressure that present peaks at about 19 and 20 s. The two modes of the flow were separated and the resulting series, named mode "*a*" (6.9–15.0 s) and mode "*b*" (21.0–29.1 s) were analyzed with Fourier and correlation methods.

Fig. 10 shows the auto spectral density functions of the velocity signals of both modes and Fig. 11, the auto spectral density functions of the respective pressure signals. None of the spectra show characteristic spectral peaks. The power densities of all signals are distinct for each mode, especially for frequencies under 200 Hz.

The cross-correlations between the pressure signal and the velocity signal of Probe "1", which is nearer the

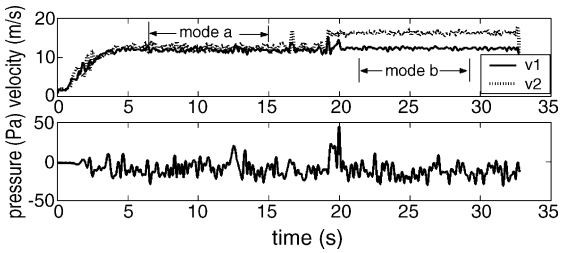

Fig. 9. Reconstructed approximations of the velocities and pressure signals, showing the separation of the series in modes "*a*" and "*b*".

pressure wall tap, are presented in Fig. 12, showing a weak correlation at mode "*a*" and an almost null correlation at mode "*b*", corroborating that the flow behavior is not alike at both modes and can not be studied at once by Fourier analysis, as if it was stationary.

The continuous wavelet spectra of the velocity signals were computed according to equation (3) and presented in Fig. 13. Any slice of the graph, parallel to frequency–energy plane, shows an instantaneous spectral energy distribution of the signal, whereas the slice parallel to time–energy plane, represents the energy oscillation along time for a chosen frequency. The unlike behavior of the signals along time is clearly seen. Until 20 s, the energy is broad distributed at the lower frequencies, which corresponds to the carrying energy larger vortices. After 20 s, where the mean velocities are larger (Fig. 9), the energy is lower at all frequencies presented. These results agree with that of Fourier spectra (Fig. 10), however at wavelet spectra

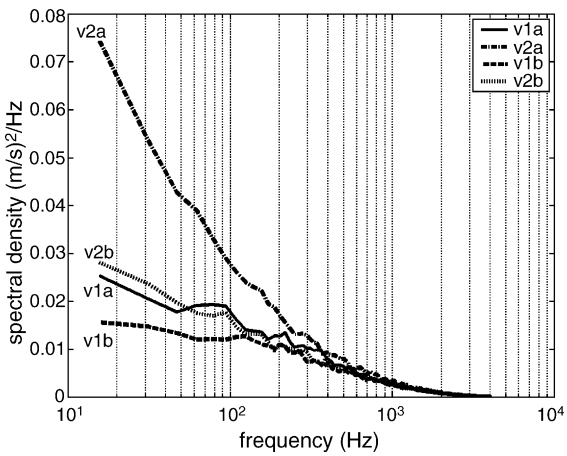

Fig. 10. Power spectral density of velocities "v_1" and "v_2" at modes "*a*" and "*b*".

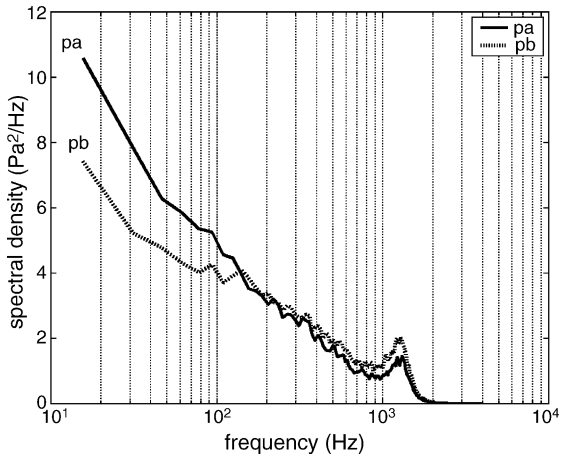

Fig. 11. Power spectral density of pressure signal at modes "*a*" and "*b*".

the analysis could be done at once, without the assumption of stationarity. Also visible is the inhomogeneous distribution of energy, remarkably at the signal of Probe "2".

Fig. 14 shows the wavelet cross-spectrum of velocity signal of Probe "1" and the pressure signal. The absolute magnitude of the wavelet cross-spectrum indicates the coherence between the signals in both frequency and time localization. The signals presented a weak coherence at the time interval corresponding to mode "*a*" and an almost null coherence at the time corresponding to mode "*b*". This is in agreement with the coherence function for the two modes, shown also in Fig. 14. Nevertheless, the strong peak at the region

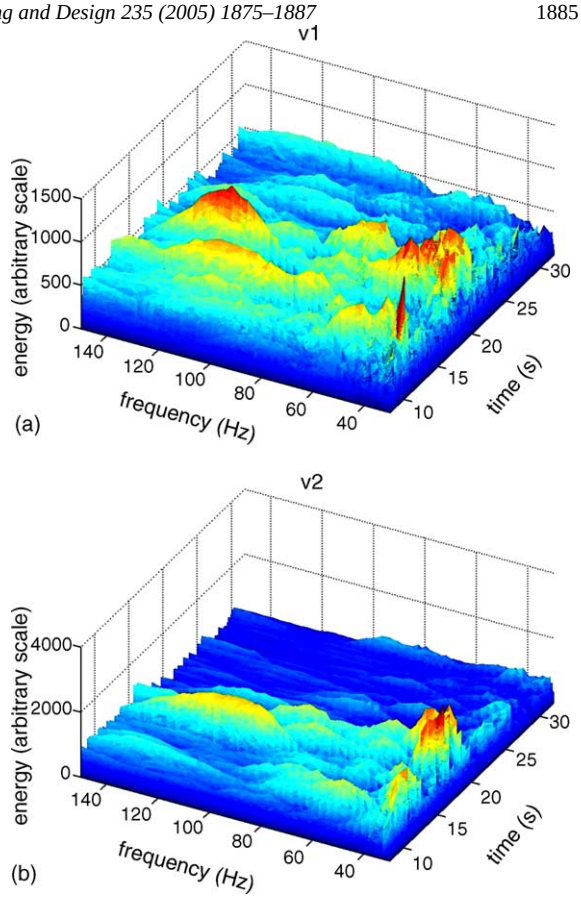

Fig. 13. Wavelet spectra of signals v_1 and v_2.

around 20 s, indicating that the transition between the two modes has good coherence between the signals, is not possible to be captured with the Fourier analysis, due to its transitory nature.

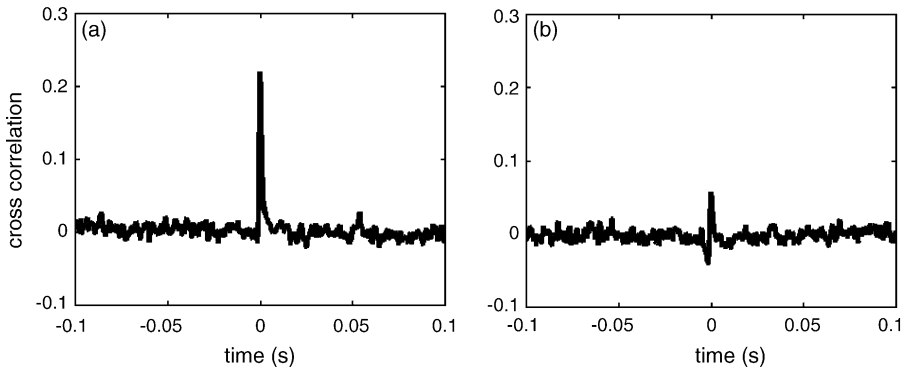

Fig. 12. Cross-correlation function of velocity v_1 and pressure at modes "*a*" and "*b*".

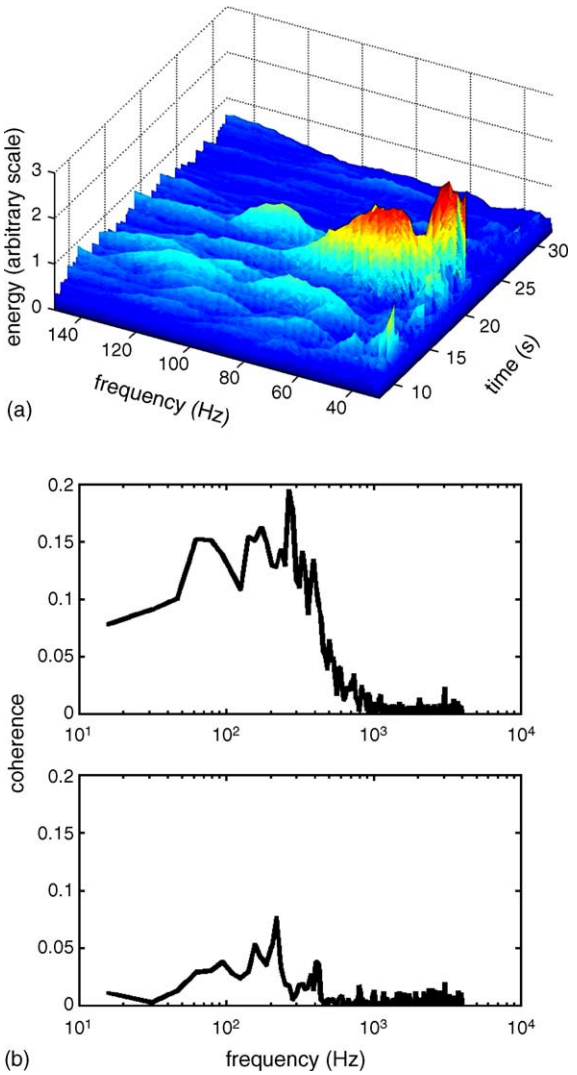

Fig. 14. Wavelet cross-spectrum of velocity v_1 and pressure signals and coherence functions of modes "*a*" and "*b*" of the same signals.

5. Concluding remarks

In this paper, the accelerating flow through a $P/D = 1.26$ tube bank is studied using hot wires and wavelet technique. The well-known wake from a cylinder perpendicular to a turbulent flow was previously studied for the comprehension of the capabilities of the wavelet tools in a multiresolution analysis context.

The property of band pass filter provided by the concurrent use of wavelet and scaling functions, in a so-called wavelet packet transform, enabled the capture of the behavior of the wake in an accelerating flow. The energy distribution could be observed at each frequency interval, with the bandwidth determined by the resolution necessary for the analysis of the phenomenon studied and by the computational resources available.

The smoothing property of wavelet decomposition and reconstruction of lower frequencies of the original transient signal was also very useful to obtain the instantaneous mean of the signal along time.

The good agreement of the transient Strouhal number in the wake of a cylinder, computed from parameters obtained in wavelet analysis with the classical stationary Strouhal number of 0.21, corroborated the proper use of wavelets for the transient turbulent wake analysis.

In the analysis of the accelerating flow through a tube bank, the wavelet technique captured the behavior on the wake region of a tube in the bank. The mode shift of the flow in both sides of the tube could be observed in the transient as well as in the steady-state flow. The intensity of the velocity fluctuations during the transient part could also be observed at several frequency intervals.

Continuous wavelet spectrum gave information about the energy distribution of the signals with time.

The wavelet cross-spectrum of velocity and pressure signals, which describes the coherence between them at time–frequency domain, and the wavelet spectra of the velocity signals, which describe their energy distribution at time–frequency domain, show undoubtedly that the flow through tube banks has a transient three-dimensional nature.

The results in this paper show also that wavelet transforms, either discrete or continuous, are very useful tools in the analysis of transient flows through tube banks, giving also valuable additional information about the flow characteristics in steady state.

Acknowledgements

Authors gratefully acknowledge the support by the Brazilian Scientific and Technological Development Council-CNPq, Grants 414216/90-3, 400180/92-8 and 520986/1997-0.

Jhon N.V. Goulart thanks also the CNPq for granting him a fellowship.

Cláudio R. Olinto thanks the CAPES, Ministry of Education, Brazil, for granting him a fellowship (PICDT-Program).

References

Blevins, R.D., 1990. Flow-Induced Vibration, second ed. Van Nostrand Reinhold, New York.

Bendat, J.S., Piersol, A.G., 1971. Random Data: Analysis and Measurement Procedures. Wiley-Interscience.

Daubechies, I., 1992. Ten Lectures on Wavelets. Society for Industrial and Applied Mathematics, Philadelphia, Pennsylvania.

Endres, L.A.M., Möller, S.V., 2001. On the fluctuating wall pressure field in tube banks. Nucl. Eng. Des. 203, 13–26.

Meyer, Y., 1993. Wavelets: Algorithms and Applications. Society for Industrial and Applied Mathematics, Philadelphia, Pennsylvania.

Ogden, R.T., 1997. Essential Wavelets for Statistical Applications and Data Analysis. Birkhäuser, Boston.

Païdoussis, M.P., 1982. A review of flow-induced vibrations in reactors and reactor components. Nucl. Eng. Des. 74, 31–60.

Percival, D.B., Walden, A.T., 2000. Wavelet Methods for Time Series Analysis. Cambridge University Press, Cambridge, UK.

Pettigrew, M.J., Taylor, C.E., Fisher, N.J., Yetisir, M., Smith, B.A.W., 1998. Flow-induced vibration: recent findings and open questions. Nucl. Eng. Des. 185, 249–276.

Rotta, J.C., 1972. Turbulente Strömungen. B.G. Teubner, Stuttgart.

Townsend, A.A., 1976. The Structure of Turbulent Shear Flow. Cambridge University Press, Cambridge, UK.

West, G.S., Apelt, C.J., 1982. The effects of tunnel blockage and aspect ratio on the mean flow past a circular cylinder with Reynolds numbers between 10^4 and 10^5. J. Fluid Mech. 114, 361–377.

Willmarth, W.W., 1975. Pressure fluctuations beneath turbulent boundary layers. Ann. Rev. Fluid Mech. 7, 13–88.

Ziada, S., Oengören, A., Bühlmann, E.T., 1989. On acoustical resonance in tube arrays. Part I: Experiments. J. Fluids Struct. 3, 293–314.